

Statistical and polarization properties of giant pulses of the millisecond pulsar B1937+21

V.I. Zhuravlev,^{1*} M.V. Popov,^{1*} V.A. Soglasnov,^{1*} V.I. Kondrat'ev,^{2,1*}
 Y.Y. Kovalev,^{1,4*} N. Bartel^{3*} and F. Ghigo^{4*}

¹*Astro Space Center, Lebedev Physical Institute, Profsoyuznaya str.84/32, Moscow 117997, Russia*

²*Netherlands Institute for Radio Astronomy, P.O. Box 2, 7990 AA Dwingeloo, The Netherlands*

³*York University, Department of Physics and Astronomy, 4700 Keele Street, Toronto, Ontario M3J 1P3 Canada*

⁴*National Radio Astronomy Observatory, P.O. Box 2, Green Bank, WV 24944, USA*

Accepted 2013 January 11. Received 2013 January 7; in original form 2012 October 31

ABSTRACT

We have studied the statistical and polarization properties of giant pulses (GPs) emitted by the millisecond pulsar B1937+21, with high sensitivity and time resolution. The observations were made in June 2005 with the 100-m Robert C. Byrd Green Bank Telescope at S-band (2052–2116 MHz) using the Mk5A VLBI recording system, with formal time resolution of 16 ns. The total observing time was about 4.5 hours; the rate of detection of GPs was about 130 per hour at the average longitudes of the main pulse (MPGPs) and 60 per hour at the interpulse (IPGPs). While the average profile shows well-defined polarization behavior, with regular evolution of the linear polarization position angle (PA), GPs exhibit random properties, occasionally having high linear or circular polarization. Neither MPGPs nor IPGPs show a preferred PA. The cumulative probability distribution (CPD) of GP pulse energy was constructed down to the level where GPs merge with regular pulses and noise. For both MPGPs and IPGPs, the CPD follows a power law with a break, the power index changing from -2.4 at high energy to -1.6 for low energy. Pulse smearing due to scattering masks the intrinsic shape and duration of the detected GPs. The smearing time varied during the observing session within a range of a few hundred nanoseconds. The measured polarization and statistical properties of GPs impose strong constraints on physical models of GPs. Some of these properties support a model in which GPs are generated by the electric discharge caused by magnetic reconnection of field lines connecting the opposite magnetic poles of a neutron star.

Key words: pulsars: general – radiation mechanisms: non-thermal – scattering – methods: data analysis – pulsar: individual: B1937+21

1 INTRODUCTION

Giant pulses from the millisecond pulsar B1937+21 were first noted by Wolszczan, Cordes & Stinebring (1984), and confirmed by Sallmen & Backer (1995). Cognard et al. (1996) determined the main properties of GPs of millisecond pulsars in their study based on 44 min of observation with the Arecibo radio telescope at 430 MHz with a time resolution of 1.2 μ s. They found that GPs were seen in both the main pulse and the interpulse components. The GPs

were found to be very short in duration. They are delayed by 40–50 μ s relative to the profile components of the regular emission, and they were highly circularly polarized, sometimes up to 100%. Cognard et al. (1996) also established a power law energy distribution with the exponent of -1.8 for the cumulative energy distribution.

Kinkhabwala & Thorsett (2000) have published results of multifrequency observations of giant radio pulses from B1937+21 observed with the Arecibo radio telescope at 430, 1420 and 2380 MHz using a time resolution of 0.38 μ s. They confirmed very short durations of GPs only restricted by the scattering time at each frequency. Although the multifrequency observations were not simultaneous, a mean radio spectrum was estimated to follow a power law with exponent $\simeq 3.1$, somewhat steeper than regular radio emission.

* E-mail: zhur@asc.rssi.ru (VIZ); popov069@asc.rssi.ru (MVP); vsoglasn@asc.rssi.ru (VAS); kondratiev@astron.nl (VIK); yyk@asc.rssi.ru (YYK); bartel@yorku.ca (NB); fghigo@nrao.edu (FG)

Popov & Stapper (2003) presented an analysis of simultaneous dual-frequency observations of GPs from PSR B1937+21, during about 3 hours with the Kalazin 64-m radio telescope at 1420 MHz, and the Westerbork Synthesis Radio Telescope (WSRT) at 2200 MHz. While more than a dozen GPs were detected at Kalazin and at WSRT, no events were found to occur simultaneously at both frequencies. Thus, the instant radio spectra of GPs are subject to deep modulation at a frequency scale of about $\Delta\nu/\nu \simeq 0.3$. Soglasnov et al. (2004) presented results of observations made at 1650 MHz with the Tidbinbilla 70-m DSS43 radio telescope with high time resolution. They have detected pulses as strong as 65000 Jy with widths ≤ 15 ns, corresponding to a brightness temperature of $T_b > 5 \times 10^{39}$ K.

In this paper we present a detailed analysis of 4.5 hours of data obtained in June 2005 with the GBT radio telescope in a 2052-2116 MHz frequency band using dual circular polarization.

In Section 2 we describe the observations and data reduction. In Section 3 we discuss our approach to calibration of polarization and we present the polarized profile of our calibrator PSR B1929+10. The average profile of B1937+21 in full polarization is described in Section 4. In Section 5 we explain the technique of GPs detection, and in the following sections we present our results on polarization (Section 6), statistics (Section 7), and scattering (Section 8). Our conclusions are summarized in Section 9.

2 OBSERVATIONS

The observations were conducted in June 2005 with the 100-m Robert C. Byrd Green Bank Telescope (GBT) at S-band (2052-2116 MHz) using a VLBI Mk5A terminal. Two polarization channels (RCP and LCP) were recorded with the following frequency setup: 2068.0 and 2100.0 MHz sky frequencies, each with USB and LSB 16-MHz subbands sampled at the Nyquist frequency (31.25 ns sampling time) with 2-bit digitizing. Thus, the configuration provided four 16-MHz conjugate bands per polarization potentially enabling 16 ns time resolution in each polarization channel. However we did not use such ultimate time resolution since scatter broadening was found to be about 100 ns, completely masking the intrinsic time shape of giant pulses (see Section 8 for details). The calibration was performed by injecting a noise diode signal with level 2.1 K, and by observations of bright continuum sources 3C286 and 3C399.1. Conversion to flux density (Jy) used noise diode amplitudes calibrated on 3C286 and 3C399.1 with flux densities from Baars et al. (1977). The System Equivalent Flux Density (SEFD) was estimated to be 11.2 Jy, and the value was used to convert our measurements to Jy throughout the paper. We believe that our flux calibration is within 10% in relative accuracy. Pulsar B1929+10 was observed several times at different hour angles for polarization calibration. Data, amounting to about 2TB total, were recorded on Mk5 diskpacks, copied to regular hard disks, and transferred to the processing site.

Data reduction started with Mk5a data decoding with the “mk5decode” routine composed by V.Kondratiev (Kovalev et al. 2005). The routine selects channels and converts 2-bit codes into floating point numbers -3, -1, +1, +3. This simple decoding was accompanied with correc-

tions for two-bit statistics by the rules originally proposed by Jenet & Anderson (1998). Such a correction is especially important in pulsar observations when a strong pulse is expected. For a strong pulse the threshold for discrimination between 1 and 3 does not correspond to a nominal 1 sigma level.

Efforts were made to remove several strong interfering signals in the radio spectra by substituting pseudo-random noise in the infected regions. The bandpass shape for each subband was individually corrected to provide a more efficient application of the predetection dispersion removal technique originally proposed by Hankins (1971). Some details of practical usage of the technique can be found in our previous publications: Jessner et al. (2010); Popov et al. (2002, 2009). Dispersion removal was carried out separately for each frequency and polarization channel (with 31.25 ns sampling time), but additional time shifts were simultaneously applied to different frequency channels, to align to the frequency of 2100 MHz. This last measure allows averaging data synchronously in all frequency channels, providing better sensitivity. The averaging became only possible after reduction of the raw data to real Stokes parameters.

3 POLARIMETRIC CALIBRATION USING PSR B1929+10

Raw observed Stokes parameters were calculated after dedispersion, using the following expressions (Jessner et al. 2010):

$$\begin{aligned} I_m &= W_r W_r + W_i W_i + X_r X_r + X_i X_i \\ V_m &= W_r W_r + W_i W_i - X_r X_r - X_i X_i \\ Q_m &= 2(W_r X_r + W_i X_i) \\ U_m &= 2(X_r W_i - X_i W_r) \end{aligned} \quad (1)$$

where W_r , W_i , X_r and X_i represent the real and imaginary components of the complex analytic signal in the RCP(W) and the LCP(X) polarization channels.

Observations of the pulsar PSR B1929+10 were used to estimate the instrumental cross-coupling terms of the GBT. The observed Stokes parameters at maximum intensity in the average profile of PSR B1929+10 are displayed in Figure 1, plotted versus parallactic angle for each frequency band.

Following the recommendations of Turlo et al. (1985) we use the following relation

$$S_{\text{obs}}(I_m, Q_m, U_m, V_m) = |M_{i,j}| S_{\text{true}}(I, Q, U, V) \quad (2)$$

It was possible to decompose the original matrix $|M_{i,j}|$ as a combination of two matrices: a time-independent matrix $|T_{i,k}|$, and a matrix $|B_{k,j}|$ describing the rotation of the telescope while tracking the radio source

$$|B_{k,j}| = \begin{vmatrix} 1 & 0 & 0 & 0 \\ 0 & \cos 2\beta & -\sin 2\beta & 0 \\ 0 & \sin 2\beta & \cos 2\beta & 0 \\ 0 & 0 & 0 & 1 \end{vmatrix} \quad (3)$$

where β is the parallactic angle. In the general case one needs to find all 16 unknown coefficients of $|T_{i,k}|$, but McKinnon (1992) simplified the procedure and reduced the number of unknown coefficients to 5. We applied the combined method of Turlo and McKinnon using our calibration

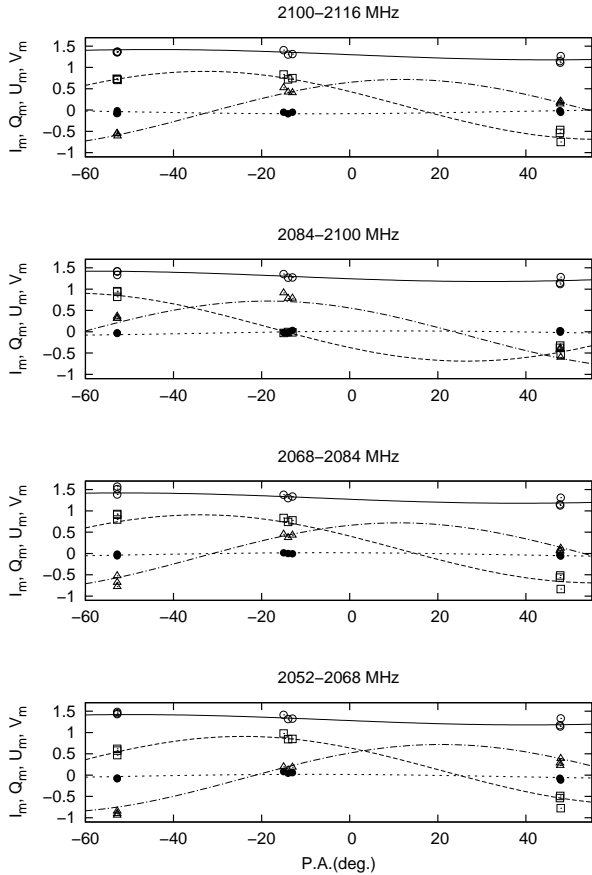


Figure 1. Measured Stokes parameters from PSR B1929+10 in four 16 MHz subbands, normalized by the invariant interval $\sqrt{I_m^2 - Q_m^2 - U_m^2 - V_m^2}$ and plotted as a function of parallactic angles. Each data point represents the average of about 300 pulsar periods. Here, I_m is denoted by open circles, Q_m by squares, U_m by triangles, and V_m by closed circles. Stokes parameters were estimated by fitting sine functions with a nonlinear least squares method. Solid, dashed, dash-dotted, dotted lines represent the approximations for I_m , Q_m , U_m , V_m correspondingly.

measurements on PSR B1929+10 presented in Figure 1. We estimate depolarization $D_p = \frac{\sqrt{T_{12}^2 + T_{13}^2}}{|T_{11}|}$, representing the linear polarization which appears as total intensity. The instrumental polarization $A = \frac{\sqrt{T_{21}^2 + T_{31}^2}}{|T_{11}|}$ represents the total intensity which appears as linear polarization. Values of D_p and A have a value of 11%. These values were found to be the same in all four frequency channels while the instrumental phases are different. A similar cross-coupling, about 6.8%, occurs between the circular and linear polarization. We do not take into account the rotation measure correction between frequency bands which constitutes only 2° . The recovered polarization profile of the PSR B1929+10 is shown in Figure 2. The profile was formed by averaging about 2800 pulses at parallactic angles of -54° , -17° , and 48° . In the frame of the rotating vector model (RVM) (Radhakrishnan & Cooke 1969) one can estimate geometric parameters of the neutron star rotation by using the PA variation curve for the main pulse and interpulse longitudes (not shown in Figure 2). The curves indicate the fits to RVM: $P.A.(\phi) = \arctan \left[\frac{\sin(\alpha) \sin(\phi - \phi_0)}{\sin(\xi) \cos(\alpha) - \cos(\xi) \sin(\alpha) \cos(\phi - \phi_0)} \right] + const$,

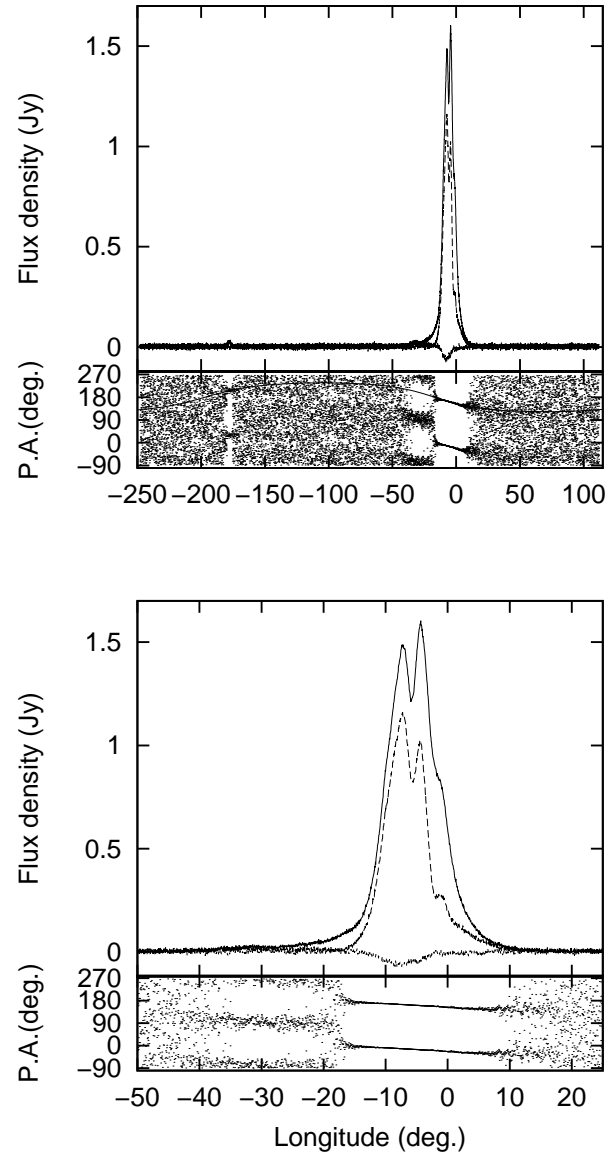


Figure 2. Pulse profiles for PSR B1929+10 after polarization calibration. The solid line represents the total intensity I , the shaded line is the linear intensity $L = \sqrt{Q^2 + U^2}$, the shaded-dotted line is the circular intensity V . The position angle $P.A. = 0.5 \arctan(U/Q)$ is plotted twice for clarity. The upper portion of the figure shows the pulse profiles for the full period of the pulsar, and the bottom one shows only the main pulse.

where α is an angle between the spin axis and the magnetic axis, β is an angle between the magnetic axis and the line of sight from Earth, and $\xi = \alpha + \beta$ is the angle between the rotation and the the line of sight. Our estimates are $\alpha = 54^\circ$ and $\beta = 43^\circ$. The profile is in good agreement with the published data (see, for example, Rankin & Rathnasree (1997)).

According to the theory of radiation transfer developed by Beskin & Philippov (2012), the mean pulse for this pulsar is formed by the extraordinary mode (the signs of the PA derivative and circular polarization are the same).

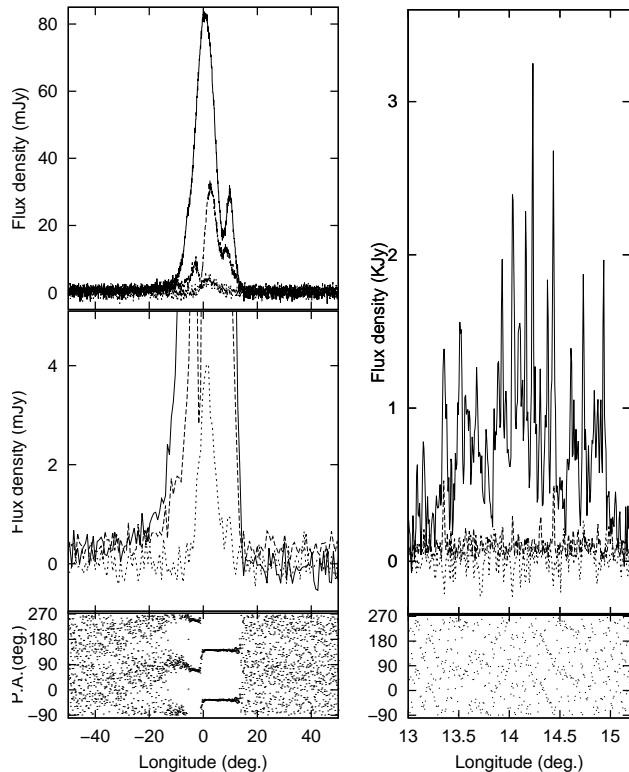


Figure 3. Regular emission (left) and averaged GPs profile (right) for the main pulse of the PSR B1937+21 after time smoothing over 312.5 ns (10 points). Full intensity – solid line, linear intensity – shaded line, and circular intensity – dotted line.

4 AVERAGE PROFILE OF PSR B1937+21

Polarization properties of the average profile for the millisecond pulsar B1937+21 were presented and discussed in several publications (Lyne & Manchester (1988); Thorsett & Stinebring (1990); Stairs et al. (1999); Kondratiev et al. (2006); Yan et al. (2011)). In our study we have the best time resolution and good sensitivity compared with the above mentioned investigations. The average polarization profile obtained in our study with the GBT at S-band is shown in Figures 3 and 4 with time resolution of 312.5 ns (10-points time smoothing), constructed by summing all four frequency bands. The ephemeris and value of the dispersion measure $DM=71.0398 \text{ pc cm}^{-3}$ were taken from Manchester et al. (2005) and corrected by the observed time of arrival of GPs ($DM=71.029 \text{ pc cm}^{-3}$).

In general our results agree with previous studies, but we would like to note some peculiarities. We confirm the nearly flat shape of PA with longitude over the major portion of the main pulse and over the full range of longitudes at the interpulse. Note, that the nearly 90-degree jump in the PA curve coincides with the sudden increase of circular polarization, and the flat portion of the PA curve covers continuously the tail of the whole main component including the second distinct component of the main pulse. In fact, the observed jump in the PA is not equal to 90 deg, but is definitely closer to 80°; this peculiarity was also found by Yan et al. (2011). We did distinguish very well the presence of an extended weak component preceding the main one.

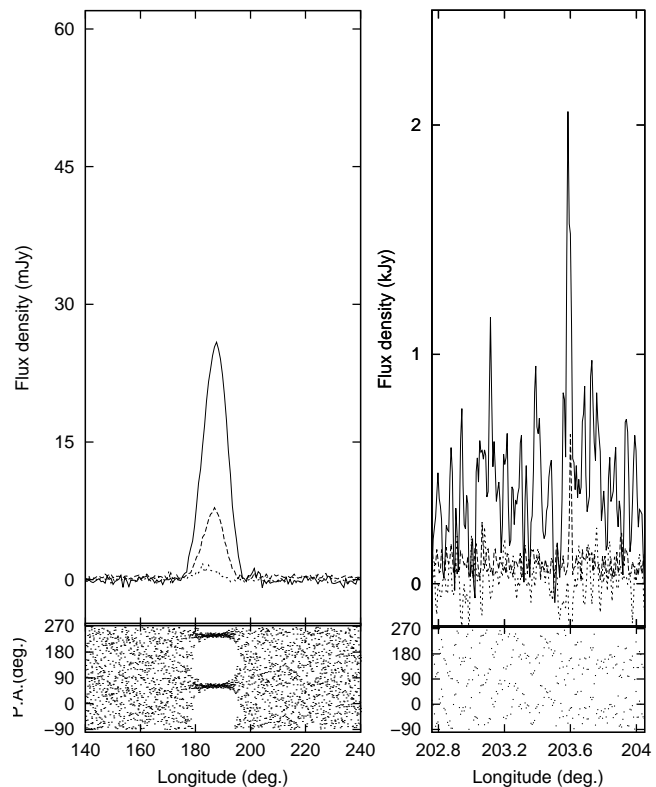


Figure 4. Regular emission (left) and averaged GPs profile (right) for the interpulse of PSR B1937+21 after time smoothing over 312.5 ns (10 points). All other details are the same as for figure 3.

It is interesting to stress that the PA curve for this pulsar is flat. According to Beskin & Philippov (2012), this is typical of millisecond pulsars, in which the polarization characteristics are formed near the light cylinder, where the magnetic field of a neutron star is close to uniform.

5 DETECTION OF GIANT PULSES

Searches for giant pulses were conducted in full intensity I averaged over all frequency bands (8 channels altogether), with the resulting root mean square deviation (RMS) of $\sigma = SEFD/\sqrt{8} = 4\text{Jy}$. Such a signal follows χ^2 statistics with 16 degrees of freedom. It is well known that GPs from the millisecond pulsar B1937+21 are very short (Soglasnov et al. 2004), but still they may have slightly different durations, and we tried several cases of time averaging by 1, 3, 5, and 7 points to get the best SNR for a given GP. For each case we applied a particular threshold for the detection. The values of the thresholds used are given in Table 1. In total there were detected 597 and 282 GPs at the longitudes close to the main pulse (MPGP) and the interpulse (IPGP) correspondingly. Time intervals between the middle of the GP window and the longitude of the maximum of the corresponding component of the average profile were found to be 59.2 and 67.3 μs , in very good agreement with the values given by Soglasnov et al. (2004) at 1650 MHz (58.3 and 65.2 μs). Therefore, there is no notable expansion in the

Table 1. GP detection thresholds for various signal times

Averaging	1	3	5	7
Duration (ns)	31.25	62.5	151.25	218.75
GP threshold in σ	13	11	10	9
GP threshold in Jy	52	25	18	13

The thresholds were calculated for the expected $\chi_P^2(\nu)$ distribution $P(\sigma_i > \sigma_{th}) = \exp(-\frac{\sigma_{th}}{2}) \sum_{j=0}^{j=\nu/2-1} \frac{1}{j!} (\frac{\sigma_{th}}{2})^j$ by the condition of $P(\sigma_i > \sigma_{th}) < 3 \cdot 10^{-13}$ resulting in less than 1% false detections in strong GPs with energies greater than 2 Jy $\cdot\mu$ s (see Section 7).

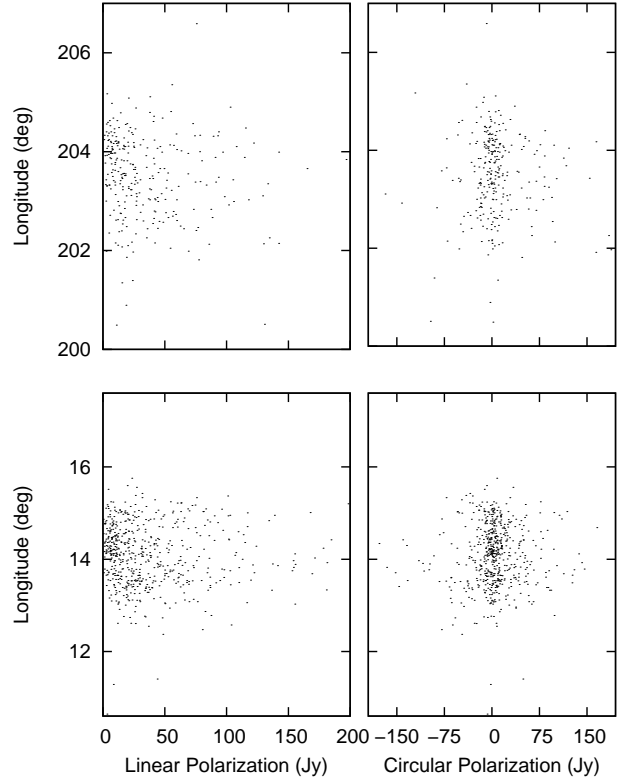
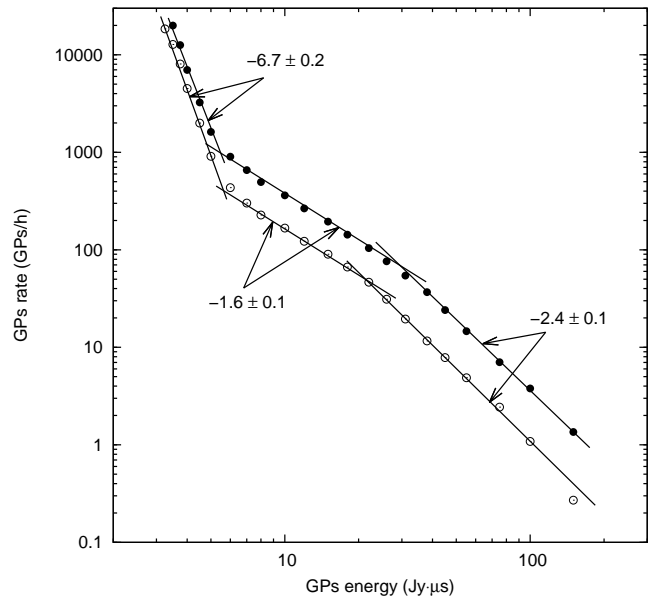
separation of regular and GP profiles between frequencies of 1650 and 2100 MHz.

6 POLARIZATION PROPERTIES OF GIANT PULSES.

Using the technique described in Section 3 we calculated corrected Stokes parameters for every frequency band. Additionally, we averaged Stokes parameters over five points near every GPs maximum. Thus every value is an average over 20 points (four in frequency and five in time). In Figures 3 and 4 we compare average profiles in full polarization for regular and GPs emission. While the regular emission shows well defined behaviors of Stokes parameters with the longitude of the average profile, profiles of GPs do not show any regular polarization. Only strong GPs (with total intensity $I_{MPGP} > 21\sigma(84Jy)$ and $I_{IPGP} > 19\sigma(76Jy)$) were used for this study. Individual GPs have high linear or circular polarization of both signs. However, there is no dependence of Stokes parameter on longitude, or on the intensity of the GPs. We have analyzed the distributions of GPs Stokes parameters, and have found them to be random. An example of longitude distribution is given in Figure 5.

7 ENERGY DISTRIBUTION

The energy of each GP was calculated as $E = \max_{N=1,3,5,7} (\delta t \sum_{i=1}^N F_i)$ with F being flux density Jy, and δt is the sampling interval (31.25 ns). We integrated over windows of 1, 3, 5 or 7 points where the GP showed the greatest SNR. To compensate for false detection at low energies, we conducted an identical calculation in the off-pulse window. Finally we subtracted the normalized number of detections in the off-pulse window from the number detected in the on-pulse window for each energy interval (for weak pulses with energy below 6 Jy $\cdot\mu$ s such corrections were essential). After these corrections the cumulative probability distribution (CPD) was obtained separately for the main pulse and the the interpulse GPs. The CPDs are shown in Figure 6. The CPDs were approximated by power law functions with different exponents in different energy ranges, the values were found to be similar for MPGPs and IPGPs. The exponent for the high energy GPs is -2.4 ± 0.1 , while the exponent for low energy GPs is -1.6 ± 0.1 . Values of the energy E_{break} are 30.2 and


Figure 5. Distributions of circular intensity (right) and linear polarized intensity (left) RPs for PSR B1937+21. Versus the longitude of pulses for main pulses (down) and interpulse (up).

Figure 6. Cumulative probability distribution of the energies of GPs in the main pulse (filled circles) and interpulse windows (open circles). Solid lines represent least-squares linear fits.

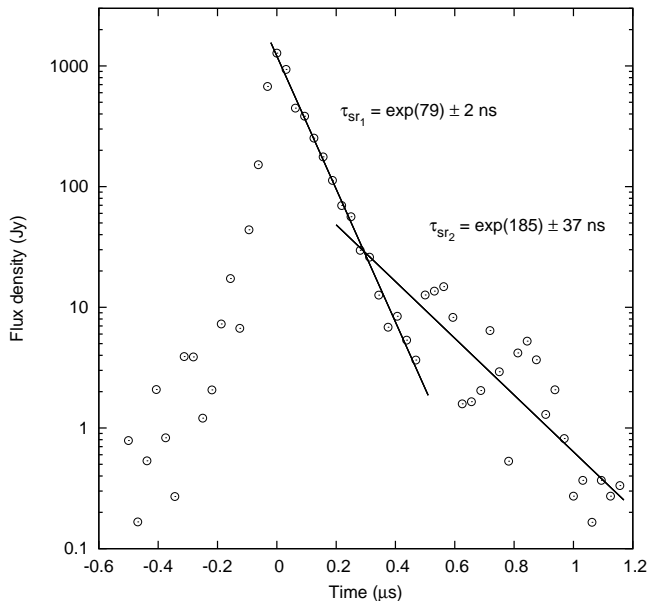


Figure 7. The profile of the strongest GP of B1937+21 (open circles). Solid lines show the least-squares fits to the exponential scattering tail of the profile, giving estimated scattering times of $\tau_{sc1} = 79 \pm 2$ and $\tau_{sc2} = 185 \pm 37$ ns.

20.1 Jy $\cdot\mu$ s for the MPGPs and IPGPs respectively. At very low energies we detected pulses of regular emission at the trailing edge of the average profile with the Gaussian distribution, where the CPDs have a fast increase.

Let us consider that the difference in E_{break} is caused by the beaming effects, i.e. we have 2/3 attenuation in IPGPs. Then we shall have the number of detections for a given flux density value $N_{IPGP} = (\frac{2}{3})^{-5/2} N_{MPGP}$ for the strong region of CPD. This is exactly the case observed.

A similar break in CPD was found by Popov & Stapper (2007) for the GPs from the Crab pulsar in their analysis of 3.5 hours of observation with the WSRT at 1200 MHz. They gave a similar explanation (beam attenuation) for the CPD peculiarities for IPGPs and MPGPs.

8 SCATTERING PARAMETERS

The scattering of radio waves is manifested in the following effects: pulse broadening, intensity variations, distortion of radio spectrum, angular broadening. To estimate pulse broadening we selected several strong GPs not showing any evident intrinsic structure, and have measured the value of τ_{sc} in the exponential tail of the pulse shape $Y(t) = Ae^{-t/\tau_{sc}}$. Figure 7 illustrates the technique. Values of τ_{sc} were measured to be 79 ± 2 and 185 ± 37 ns. While the short time-scale is based on the pulse portion with good signal-to-noise ratio ($SNR > 10$), the long time scale was estimated in the portion of the pulse merging with noise ($\sigma = 4$ Jy), but we consider it to be real since the approximation was done over about 1 μ s time interval, thus providing averaging with the resulting σ near 1 Jy. The pulse broadening time τ_{sc} must be correlated with the decorrelation bandwidth $\Delta\nu_d$ in the radio spectrum through the relation $2\pi\tau_{sc}\Delta\nu_d = C$ with C being a constant close to 1.0. With this relation we

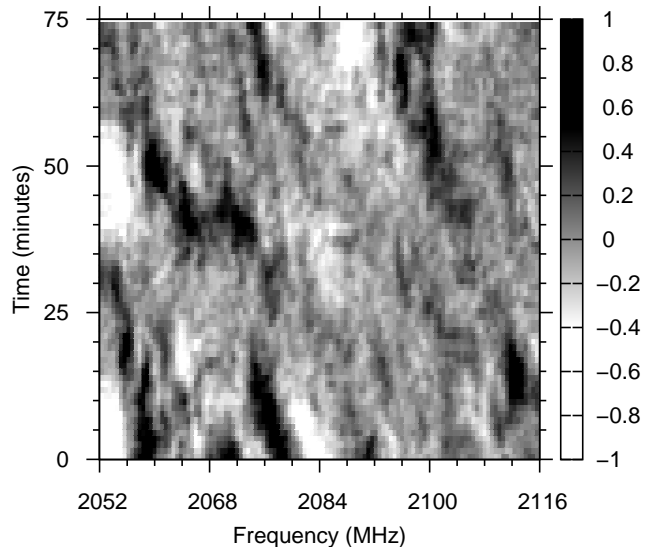


Figure 8. Dynamic spectra of selected observation data with high GP activity.

can expect to find two frequency scales for $\Delta\nu_d$ of about 2 MHz and 0.85 MHz in the radio spectrum. To measure the $\Delta\nu_d$ we constructed the dynamic spectrum over the total 64 MHz band (B). The border regions between conjugate 16 MHz sub-bands were filled with random noise with corresponding mean value and variance. The example of such a dynamic spectrum is presented in Figure 8. To obtain values for scintillation bandwidth and scintillation time we use a 2-dimensional autocorrelation function (ACF) of the dynamic spectrum. Frequency and time sections were approximated by a combination of Gaussians. It was found that there are three frequency scales in the diffraction pattern with $\Delta\nu_{d1} = 2220 \pm 20$, $\Delta\nu_{d2} = 690 \pm 15$ and $\Delta\nu_{d3} = 110 \pm 5$ kHz at a half width level. For the region of low activity the scintillation time Δt_{sc} was fitted with only one Gaussian ($\delta t_{sc} = 6$ min), and two components ($\delta t_{sc} = 7$ and 2 min) were found for the region of high activity. The results are presented in Table 2.

If we disregard the multiple frequency structure, we can use the value of $\Delta\nu_d = 1.7$ MHz. With this value of $\Delta\nu_d$ we have a scintillation intensity modulation in the total $B = 64$ MHz band being significantly reduced ($\Delta\nu_d/B = 0.025$). Therefore our analysis of energy distribution was not affected by the scintillations.

We noticed two time intervals of GP activity that may be connected with scintillation effects. The region of high activity was about one hour duration, and the region of low activity was about three hours.

9 DISCUSSION AND CONCLUSIONS

Let us review our findings:

1) The observed durations of GPs from PSR B1937+21 reflect mainly scatter broadening of about 100 – 200 ns, while the intrinsic time width was unresolved ($\lesssim 30$ ns).

2) Our analysis of polarization properties of GPs revealed random behavior of polarization with occasional pulses showing high linear polarization as well as high circu-

Table 2. Amplitudes and widths for time and frequency sections of the ACF of dynamical spectra for two stages of activity GPs. (Only statistical fitting errors are given.)

	Time scales	
	Region of high activity	Region of low activity
$A_1 \cdot 10^{-3}$	63.4 ± 0.2	103.3 ± 0.6
$A_2 \cdot 10^{-3}$	14.7 ± 0.2	
Δt_{sc1} (min)	7.1 ± 0.8	6.1 ± 0.5
Δt_{sc2}	2.1 ± 0.4	
	Frequency scales	
	Region of high activity	Region of low activity
$A_1 \cdot 10^{-3}$	57.0 ± 0.5	52.1 ± 1.5
$A_2 \cdot 10^{-3}$	15.3 ± 0.6	39.0 ± 1.5
$A_3 \cdot 10^{-3}$	6.2 ± 0.8	12.5 ± 0.5
$\Delta \nu_{d1}$ (kHz)	2220 ± 20	3650 ± 60
$\Delta \nu_{d2}$	690 ± 15	1740 ± 30
$\Delta \nu_{d3}$	110 ± 5	500 ± 10

lar polarization of both signs, in contrast to the average profile of regular radio emission. Such polarization properties impose strong constraints for theoretical models explaining physical nature of GPs.

3) The cumulative probability distribution in energy was obtained based on a large volume of statistical data down to $3 \text{ Jy} \cdot \mu\text{s}$. The CPD demonstrated that there is no cutoff at low energies, i.e. the weakest GPs merge smoothly with the regular component of radio emission.

4) The CPD has a definite break in the power law exponent at energies equal to 30.2 and 20.1 $\text{Jy} \cdot \mu\text{s}$ for the MPGPs and IPGPs respectively. At these energies the exponent changes its value from -1.6 ± 0.1 to -2.4 ± 0.1 , i.e. approximately by -1 . The same behavior was found for the CPD Crab pulsar GPs, as published by Popov & Stapper (2007). Thus, an observed break in the exponent of the power law dependence of the CPD seems to be intrinsic to the mechanism of the generation of giant radio pulses.

The above mentioned properties fit very well the explanation given by Istomin (2004) in his model of origin of GPs as a result of the reconnection of the last open/close magnetic field line (MFL). In a case of nearly perpendicular rotation (magnetic axis is perpendicular to the axis of rotation) the last open MFL, when reconnected, will join regions of the polar caps with different signs of electric potential ψ thus leading to a strong electric discharge and plasma particle creation and acceleration. Istomin proposes specific maser amplification of plasma waves induced by a two-stream instability. The model expects large circular components in polarization of GPs. What is interesting, Istomin's model predicts a power law dependence for the CPD with the exponent $-3/2$ or $-5/2$ depending on the power density of plasma generated inside the discharge tube. Thus, such a transition from one energy state to another may be accompanied by a break point in CPD.

ACKNOWLEDGMENTS

This work was based on GBT observations conducted within the project GBT05B-038. Our study was supported by the Russian Foundation for Basic Research (project code 10-02-0076) and the Basic Research Program of the Presidium of the Russian Academy of Sciences on "The Origin, Structure, and Evolution of Objects in the Universe". The National Radio Astronomy Observatory is a facility of the National Science Foundation operated under cooperative agreement by Associated Universities, Inc. At the time of observations Y.Y. Kovalev was an NRAO Karl Jansky fellow. We thank V. Beskin and Ya. Istomin for helpful discussion.

REFERENCES

- Baars J.W.M., Genzel R., Pauliny-Toth I.I.K., Witzel A., 1977, A&A, 61, 99
- Beskin V.S. & Philippov A.A., 2012, MNRAS, 425, 814
- Cognard I., Shrauner J.A., Taylor J.H., Thorsett S.E., 1996, ApJ, 457, L81
- Hankins T.H., 1971 ApJ, 169, 487
- Istomin Ya.N., 2004, Young Neutron Star and Their Environment, IAU Symposium, Vol. 218, 369
- Jenet F.A., Anderson S.B., 1998, PASP, 110, 1467
- Jessner A., Popov M.V., Kondratiev V.I., Kovalev Y. Y., Graham D., Zensus A., Soglasnov V.A., Bilous A.V., Moshkina O.A., 2010, A&A, 524, 60
- Kinkhabwala A. & Thorsett S.E., 2000, ApJ, 535, 365
- Kondratiev V.I., Popov M.V., Soglasnov V.A., Kovalev Y.Y., Bartel N., Ghigo F., 2006, in Becker W., Huang H.H., eds, Proceedings of the 363, WE-Heraeus Seminar on: "Neutron Stars and Pulsars",
- Kovalev Y.Y., Ghigo F., Kondratiev V.I., Bartel N., Soglasnov V.A., Popov M.V., 2005, NRAO GBT Memo Ser. 236, 20p
- Lyne A.G. & Manchester R.N., 1988, MNRAS, 234, 477
- Manchester R.H., Hobbs G.B., Teoh A., Hobbs M., 2005, AJ, 129, 1993
(<http://www.atnf.csiro.au/research/pulsar/psrcat/>)
- McKinnon M.M., 1992, A&A, 260, 533
- Popov M.V., Bartel N., Cannon W.H., Novikov A. Yu., Kondratiev V.I., Altunin V.I., 2002, A&A, 396, 171
- Popov M.V. & Stapper B. 2003. ARep, 47, 660
- Popov M.V. & Stappers B., 2007, A&A, 470, 1003
- Popov M., Soglasnov V., Kondratiev V., Bilous A., Moshkina O., Oreshko V., Ilyasov Y., Sekido M., Kondo T., 2009, PASJ, 61, 1197
- Radhakrishnan V., & Cooke D.J., 1969, Astrophys. Lett., 3, 225
- Rankin J.M., & Rathnasree N., 1997, J. Astrophys. Astron., 18, 91
- Sallmen S. & Backer D.C., 1995, in Fruchten A.S., Tavani M, Backer D.C., eds, Millisecond Pulsar. A decade of Surprise, held in Aspen, Colorado, Jan. 3-7. ASPC Ser. Vol. 72, Publ. Astron. Soc. Pac., San Francisco, p. 340
- Soglasnov V.A., Popov M.V., Bartel N., Cannon W., Novikov A.Yu., Kondratiev V.I., Altunin V.I., 2004, ApJ, 616, 439
- Stairs I.H., Thorsett S.E., Camilo F., 1999, Astrophys. J. Supplem. Ser., 123, 627

- Thorsett S.E. & Stinebring D.R., 1990, *Astrophys.J.*, 361, 644
- Turlo Z., Forkert T., Sieber W., Wilson W., 1985, *A&A*, 142, 181
- Yan W.M., Manchester R.N., van Straten W. et al., 2011, *MNRAS*, 414, 2087
- Wolszczan A., Cordes J., Stinebring D. 1984, In *Millisecond Pulsars*, ed. by S.P.Reynolds and D.R. Stinebring (Green Bank: NRAO) p.63

This paper has been typeset from a \TeX / \LaTeX file prepared by the author.